Available online at www.sciencedirect.com

ScienceDirect

Procedia CIRP 117 (2023) 293–298

www.elsevier.com/locate/procedia

19th CIRP Conference on Modeling of Machining Operations

Simulation of local contact conditions in the secondary shear zone in dry and wet metal cutting

B. Denkena[a], H.C. Liu[b,c,d], F. Pape[b], B. Bergmann[a], G. Poll[b], J. Schenzel[a], L. Ellersiek[a]*

[a]*Institute of Production Engineering and Machine Tools (IFW), Leibniz Universität Hannover, An der Universität 2, 30823 Garbsen, Germany*
[b]*Institute of Machine Design and Tribology (IMKT), Leibniz Universität Hannover, An der Universität 1, 30823 Garbsen, Germany*
[c]*State Key Laboratory of Solid Lubrication, Lanzhou Institute of Chemical Physics, Chinese Academy of Sciences, 730000 Lanzhou, China*
[d]*Qingdao Key Laboratory of Lubrication Technology for Advanced Equipment, Center of Resource Chemistry and New Materials, 266100 Qingdao, China*

* Corresponding author. Tel.: +49-511-762-18234; fax: +49-511-762-5115. *E-mail address:* ellersiek@ifw.uni-hannover.de

Abstract

Cutting fluids significantly influence the contact conditions in metal cutting, e.g. stresses or contact areas. Due to the limited accessibility of the chip-tool contact, the identification of contact conditions is challenging. In this paper, a simulation model is created and used to identify the real contact area in dry and wet cutting. Experimentally identified normal stresses and chip-tool roughness serve as input parameters. The results show higher normal stresses in wet cutting, which results in a higher real contact area between rake face and chip.

Keywords: Metal cutting, cutting fluids, chip-tool contact, real contact area, surface roughness

1. Introduction

Cutting Fluid (CF) plays an important role during the machining of hard-to-cut materials. In many cases, the most important function of CF is the reduction of thermal loads and subsequent the reduction of wear on the tool [1, 2]. Moreover, CF also affects the mechanical loads in cutting. However, most investigations concerning mechanical loads only focus on globally averaged values [3].

The identification of local stress states is possible with several approaches, e.g., split tool [4, 5], tool with restricted contact length [6] or stress sensitive tool materials [7]. All these approaches have changes in tool geometry or tool properties in common. Therefore, they might influence the penetration and lubrication behavior of the CF. A method to calculate normal and tangential stresses based on process force and contact length measurements is proposed by Bergmann [8, 9]. The method was used to show the influence of the cutting edge rounding on the normal and tangential stresses in dry cutting.

The tribological conditions at the chip-tool interface are very complex. While the apparent contact area can be estimated by the contact length, the real contact area is determined by the asperities of the two surfaces and the normal and tangential stresses [10, 11]. The normal loads significantly influence the real contact area between the chip and the rake face, which determines the local shear stress, adhesion and heat generation. Cutting experiments with different tool roughness show the influence of local scale asperities on the cutting forces [12]. However, in cutting simulation, the roughness on the chip and tool surfaces has seldom been considered. To some extents, the local contact and friction conditions limit the accuracy of the friction modelling and hence the chip formation. If the contact conditions are characterized by capillaries, the penetration of CF in the secondary shear zone might be favor as stated in [13].

10.1016/j.procir.2023.03.050

In this paper, as a first attempt to model the surface roughness effect for the chip-tool contact, an indentation contact model has been developed to determine the real contact area. The stress calculation method presented in [8, 9] is used to calculate the normal stress distribution along the cutting wedge in dry and wet cutting. Thereafter, the normal stresses are used to determine the real contact area between the rough chip surface and the rake face numerically.

2. Experimental setup

Cutting experiments were performed on a planing test rig (Fig 1a). The test rig enables high-speed recordings and process force measurements of dry and wet cutting processes with cutting speeds up to 500 m/min and CF pressures up to 70 bar. For high-speed recordings, a Photron Fastcam SA5 was used. For the process force measurements, a dynamometer Kistler 9257B was used. The setup of the planing test rig is shown in Fig 1a. A housing, a sapphire glass and the nozzle holder protect the high-speed camera and the components of the test rig against the CF. The nozzle has a diameter of 1 mm. The CF supply is realized by an accumulator system. A detailed description of the test rig and the CF supply system can be found in [14].

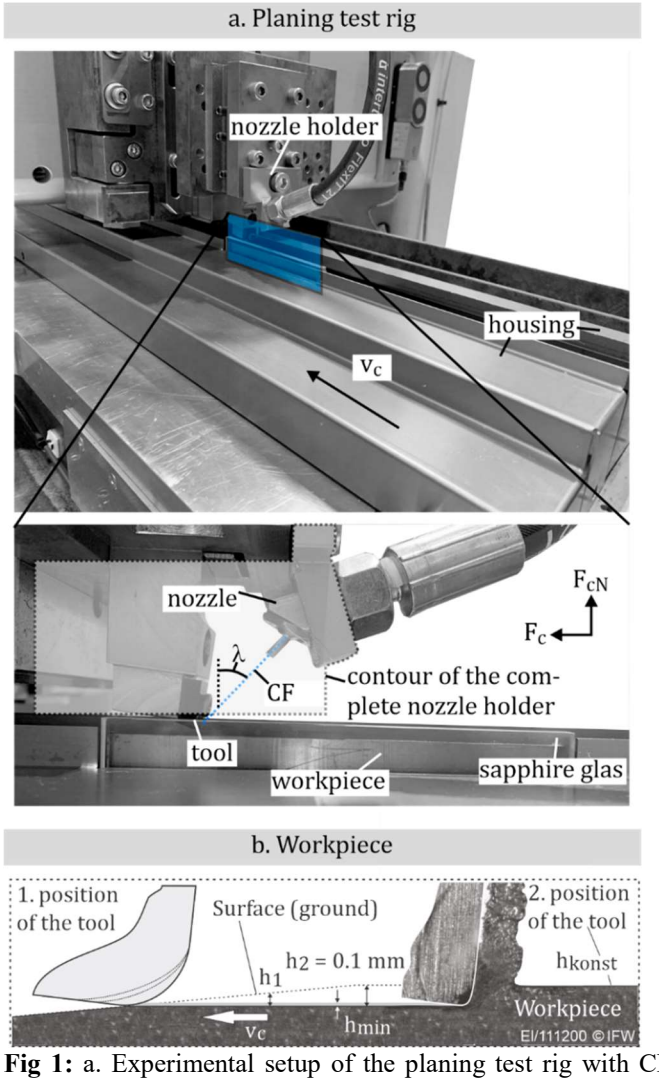

Fig 1: a. Experimental setup of the planing test rig with CF supply [14], b. Workpiece geometry [9]

Quenched and tempered steel AISI4140+QT was used as workpiece material. The workpiece geometry has a first section with an increasing height of 3 µm/mm and a section with constant height with a length of at least 53.33 mm (Fig 1b). This means that the undeformed chip thickness h increases from h = 0 mm to h_{max} = 0.1 mm in one cut. It allows the correlation between the undeformed chip thickness, the process forces and the contact length on the rake face. All processes were performed with a chip width b = 2 mm and a cutting speed v_c = 120 m/min. A TiAlN coated cemented carbide insert with symmetric cutting edge rounding $\bar{S}$ = 35 µm (SNMA120408 geometry) was used as tool. Rake and clearance angle are γ = 1° and α = 14°, respectively. Ester oil based CF Blaser Vascomill CSF35 was used as CF. The CF was supplied to the process with pressures of 10 and 30 bar and a tilt angle of λ = 40°. In addition, a dry process was performed.

3. Results of the cutting experiments

The paper focuses on the contact conditions on the rake face. To estimate normal stress distribution according to [8, 9], the contact length as well as process forces dependent on the undeformed chip thickness h, are of high importance. The time resolved process forces as well as the contact length at h = 0.1 mm are shown in Fig. 2 for dry and wet cutting processes.

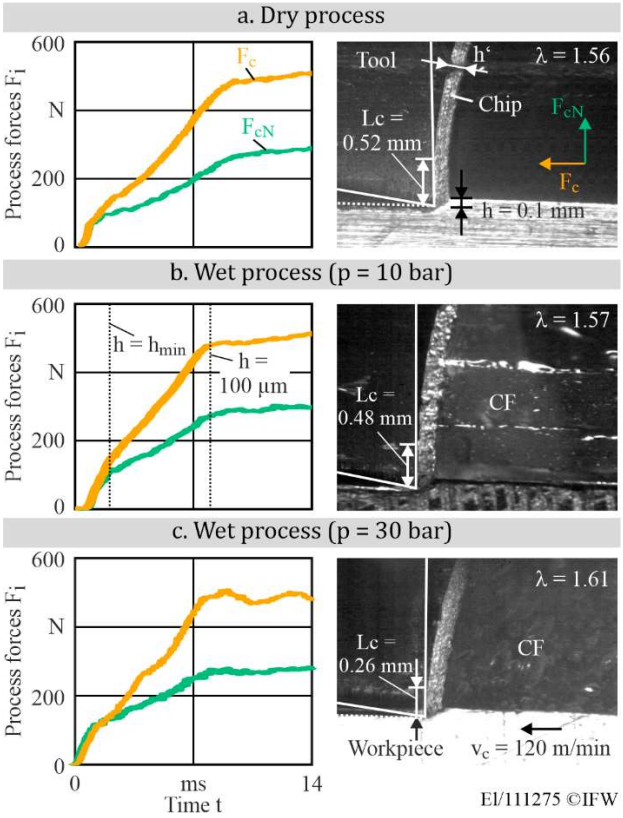

Fig 2: Time-resolved process forces and contact lengths at h = 0.1 mm a. dry process, b. p = 10 bar CF pressure, c. p = 30 bar CF pressure

The process forces are similar for all cutting processes. After the first contact between tool and workpiece, the process is characterized by ploughing effects and the cutting force F_c as well as the cutting normal force F_{cN} increase significantly.

When the undeformed minimum chip thickness h_{min} is exceeded, the chip formation begins. The slope of the two force components decreases, and the cutting force F_c distinctly exceeds the cutting normal force F_{cN}. When the maximum chip thickness of h = 0.1 mm is reached, the process forces are nearly constant, indicating a steady state of mechanical load conditions. The process forces at this point are in the same range for all processes. As a contrast, the chip formation changes significantly by the application of CF. The dry process is characterized by the longest contact length Lc = 0.52 mm. By the application of CF with pressure p = 10 bar, the contact length is reduced. The lowest contact length Lc = 0.26 mm was measured at the highest CF pressure p = 30 bar. This can be attributed to the mechanical loads of the CF acting on the chip surface [14]. The chip compression ratio λ =h'/h, on the other hand, does not vary significantly.

To calculate the normal stresses along the cutting wedge, the tool is separated into three sections (Fig 3a). A detailed description of the calculation approach is given in [8, 9].

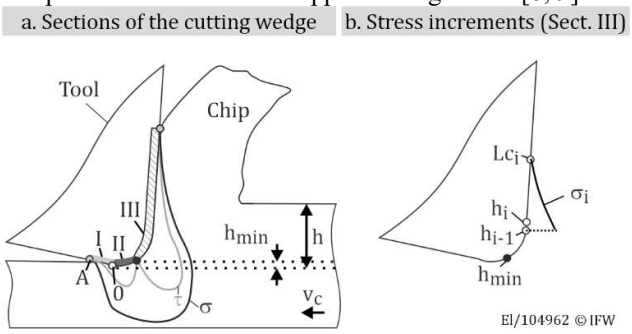

Fig 3: a. Separation of the tool in different sections b. Stress increments for the calculation of stresses in section III [8, 9]

Section I is defined from point A to point 0. The stresses in this section are characterized by a linear increase as a result of material springback. Section II is defined from point 0 to the point of the undeformed minimum chip thickness h_{min}. The stresses are constant in this section. The calculation of the stresses in section I + II is based on process force measurements at $h = h_{min}$. Section III represents the secondary shear zone on the rake face. The stresses are calculated using incremental process forces with an increasing undeformed chip thickness $\Delta h = h_{i-1} - h_i = 0.001$ mm. The incremental process forces are related to the area between chip thickness h_{i-1} and contact length Lc_i corresponding to h_i (Fig 3b). Finally, all stress increments are summarized. The results of the calculated stress for a dry process and two wet processes are given in Fig 4.

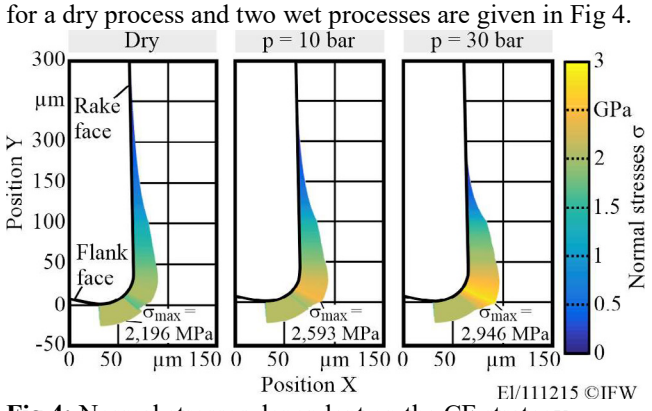

Fig 4: Normal stresses dependent on the CF strategy

It is shown that the maximum normal stress is increased by the application of CF. This can be attributed to the reduced contact length. In contrast, the process forces only change slightly by the application of CF. While the stress is very high at locations close to the cutting edge, it reduces significantly for positions $Y > h = 100$ µm. This might benefit the penetration of the CF into the secondary shear zone due to a lower real contact area between chip and rake face.

4. Simulation of the real contact area

In this section, the rough surface contact between the chip and the tool in the secondary shear zone is modeled. The real contact area is shown at different contact pressures and temperatures. This would provide some fundamental insight into the local contact conditions in the chip-tool contact zone, and may provide fundamental knowledge on further modelling of the microscopic friction, heat generation at asperity levels and thus the macroscopic friction and chip formation.

4.1 Problem definition and simplification

In principle, the chip-tool contact should be modeled as a thermal elastic-plastic contact problem with proper boundary conditions, as well as possible (boundary, mixed, fluid) lubrication effects depending on the CF penetration. As a preliminary research progress, the rough contact is the main concern in this work, and it is modeled as a plain-to-plain contact under conditions of isothermal elastic deformation at steady state. The problem is simplified to a rigid circular punch in contact with a rough plain surface. The rigid punch represents the cutting tool with a high elastic modulus showing negligible deformation, while the rough plain surface represents the interacting chip surface. A schematic representation of the contact is given in Fig 5. A circular punch is chosen since it distinctly simplifies the calculation (Sec. 4.2). Even though the entire macroscopic contact area between chip and tool might be rectangular, the focus of the simulation lies only on a small area with local contact conditions. Thus, the shape of the punch is not relevant in the current investigation. Punch radius a is chosen as 36 µm. This enables the measured roughness to coincide with the mesh used in the calculation.

No lubrication effect is modeled, and only dry contacts are analyzed, as investigations show only slight reduction of the friction coefficient for processes with CF [14]. Especially the chip movement might challenge the penetration of CF into the secondary shear zone.

4.2 Governing equations for dry rough contacts

The geometry of the rigid circular punch of radius a reads

$$h_{tool}(x,y) = \begin{cases} h_0, \text{if } x^2 + y^2 \le a^2 \\ \infty, \text{otherwise} \end{cases} \quad (1)$$

where h_0 is the punch depth, which is to be determined with the load balance equation, Eq.(4).

The gap height h between the two rough contacting surfaces can be expressed as

$$h(x,y) = h_0 + u_g(x,y) + u_{tool}(x,y) + u_{chip}(x,y) \quad (2)$$

where u_g the deformation of surfaces. u_{tool} and u_{chip} are the roughness of the tool and the chip, respectively.
Within the framework of elastic deformation, u_g can be obtained based on the half-space assumption [15] as following

$$u_g(x,y) = \frac{2}{\pi E'} \int_{-\infty}^{+\infty} \int_{-\infty}^{+\infty} \frac{p(x',y')dx'dy'}{\sqrt{(x-x')^2+(y-y')^2}} \quad (3)$$

where p is the local pressure and E' is the reduced elastic modulus of the two bodies, $E' = 2.0/\left(\frac{1-\nu_1^2}{E_1} + \frac{1-\nu_2^2}{E_2}\right)$. E_1, E_2, ν_1 and ν_2 are the elastic moduli and the Poisson's ratios of the two bodies, i.e. chip and tool respectively. The summation of the pressure must support the applied load w, which is expressed by the force balance equation

$$\iint p(x,y)dxdy = w. \quad (4)$$

The load w can be estimated by the normal stress σ in Sec. 3 multiplied with the apparent contact area. The following complementary condition between gap height and pressure should be satisfied in the complete computational domain.

$$p(x,y)h(x,y) = 0 \quad (5)$$

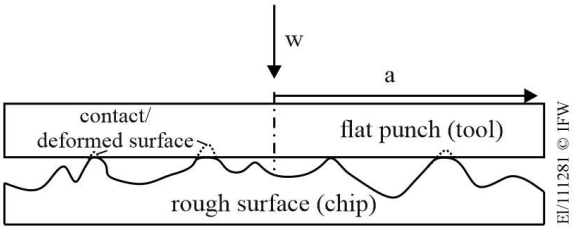

Fig 5: Schematic representation of the simulation model

4.3 Numerical solution

The above governing equations are solved in dimensionless forms. The dimensionless parameters are punch dimension and characteristic parameters p_0 and h_{ref} referred to [15]. They are

$$\overline{X} = \frac{x}{a}, \overline{Y} = \frac{y}{a}, \ \overline{P} = \frac{p}{p_0} = \frac{p}{w/(2\pi a^2)}, \ \overline{H} = \frac{h}{h_{ref}}, \quad (6)$$
$$\bar{u} = \frac{u}{h_{ref}}, \ h_{ref} = ap_0/E'.$$

The dimensionless equations are given in Appendix A. Numerically, the computation of the double integral in Eq. (3) is very expensive. To save computational time when using a dense mesh, efficient numerical methods such as multilevel multi-integration (MLMI, multigrid) method [16, 17] and fast Fourier transform method [18, 19] have been developed and widely used in the tribology community. These methods reduce the computational complexity from N^2 to $N \cdot \log N$, where N is the number of nodes in one computational direction. Here we choose the MLMI method following the approach pioneered by Venner and Lubrecht [17].

4.4 Simulation results

4.4.1 Measured chip surface

$u_{chip}(x,y)$ and $u_{tool}(x,y)$ in Eq. (2) represent the microgeometry of the chip and the tool. Since the roughness of the tool is much smaller than that of the chip, only the roughness of the chip is considered in the current simulation.

The roughness is measured by a laser scanning microscope. The resolution in the x and y directions is 140.845 nm/pixel. Fig 6a shows the measured chip surface. Note that the chip roughness does not necessarily equals the chip roughness in the chip tool contact in the section close to the cutting edge due to high normal loads and subsequent plastic deformations.

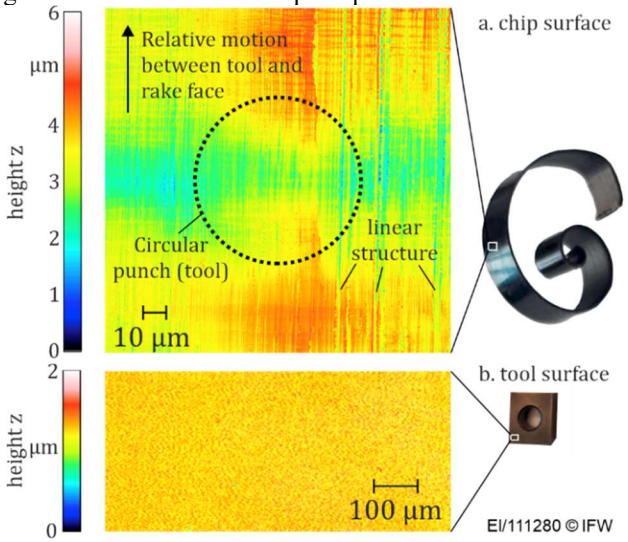

Fig 6: a. Flattened measured chip surface (1025 x 1025 points, 144.23 µm x 144.23 µm, dry cutting), b. tool surface

In general, comparable chip surfaces were generated in wet and dry cutting. The circle indicates the indentation zone by the circular punch. The chip is characterized by linear structures, which are causes by the cutting edge roughness. Moreover, a valley exists in the middle of the measured area. In addition, Fig. 6b shows the surface of the polished tool rake face. The roughness is much lower than that of the chip, and therefore the simplification of a smooth tool surface is acceptable.

4.4.2 Setting of the solver

The simulation depicts the experimental investigations in Sec. 3. Material and mechanical properties of AISI4140+QT are used for the rough surface (chip). The elastic modulus of the chip at 20 °C and 700 °C are E = 210 GPa and E = 65 GPa, respectively, according to [20], while the Poisson's ratio is assumed to be 0.3 independent of the temperature. The temperature of 700 °C is chosen based on literature for machining of steel [9]. 20 °C is chosen for comparison. For the multigrid and MLMI methods, the computation domain is -2 to 2 in x and y direction. A rectangular mesh with equal distance in the two directions is adopted. It is 5 level of grids with 1025 x 1025 nodes on the highest level, which coincide the measured roughness without interpolation. 32 W cycles are performed before output. The initial pressure distribution is assumed as

$$p(x,y) = \begin{cases} p_0/\sqrt{1-(x/a)^2-(y/a)^2}, \text{if } x^2+y^2 \le a^2 \\ 0, \text{otherwise} \end{cases} \quad (7)$$

4.4.3 Typical results of footprint of contact

The calculated real contact area at different contact pressures and temperatures is shown in Fig 7 and Fig 8. The mean contact pressure is chosen in three steps based on the results in Sec. 3 (Fig 4). The lowest mean normal contact pressure chosen is 0.3 GPa, which occurs at the end of the contact length between chip and rake face. The second mean normal contact pressure is 1 GP. This contact pressure occurs approximately at Y = h = 0.1 mm in Fig. 4. The highest normal

contact pressure is 3 GPa, which corresponds to the highest normal stress calculated in Sec. 3 for wet cutting with CF pressure p = 30 bar. These three pressure values cover most of the range of pressures encountered in the chip-tool contact in dry and wet cutting. By looking at the changes of the contact conditions with increasing contact pressure, knowledge about the influence of the CF on the contact conditions can be gained. The percentage of the real contact area is determined by the ratio of the local mesh points with pressure to the whole number of grid points in the apparent circular contact region.

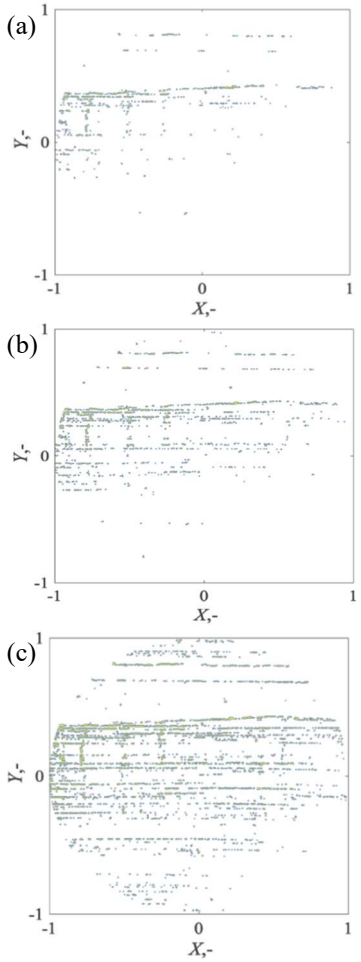

Fig 7: Calculated real contact zone between a rigid flat (circular) tool and rough chip surface at 20 ℃. (mean contact pressure: a. 0.3 GPa; b. 1.0 GPa; c. 3.0 GPa)

The simulated results for 20 °C are shown in Fig 7. The colored points indicate a contact between chip and tool. It can be seen that the contact area increases significantly with increasing mean contact pressure. The percentage of the contact area is 0.4%, 1.0%, and 2.6%, respectively. The contact areas match with the linear structures of the chip surface. The valley of the measured surface does not seem to have a significant influence on the contact area. Compared with Fig 8 at 700 °C, it is noticeable that the real contact area increases at a higher temperature due to softening of the chip and the reduced elastic modulus E. However, the maximum real contact area is limited to 8.5% for the used highest pressure of 3 GPa and temperature of 700 ℃, i.e. the case in Fig 8(c). Thereby, it should be noted that the simulation is based on several assumptions, e.g. a pure elastic material behavior and a flat tool surface. For high normal pressures those assumptions might be invalid. Nevertheless, basic relationships are shown by the simulation. Since higher normal stresses were demonstrated for wet cutting, a higher contact area between tool and chip is expected. Nevertheless, the majority of the contact zone seems unloaded and the resulting gaps may serve as micro-channels for CF penetration depending on the cutting speeds and dynamics. Moreover, for a precise prediction also the exact temperature in cutting has to be considered.

Another aspect that is influenced by the real contact area is the tool wear. Wet processes are associated with higher normal loads, which results in a higher real contact area and therefore in higher wear rates according to Usui [21]. However, the wear reduction due to the application of CF is shown in many cases. This underlines the importance of cooling effects of the CF, since lower temperatures reduce the wear rate [21].

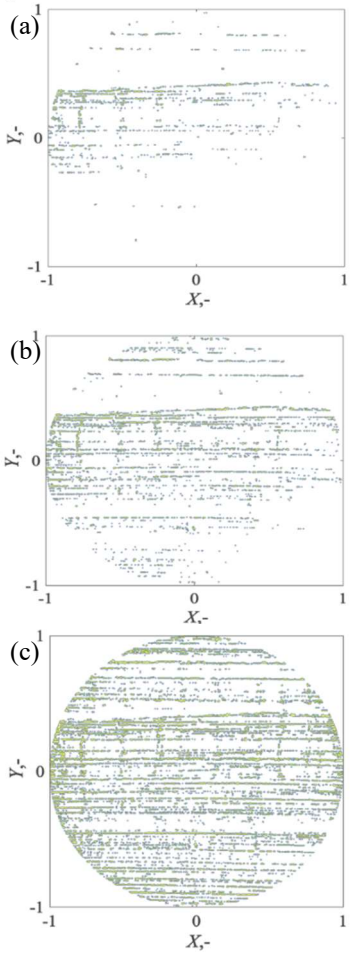

Fig 8: Calculated real contact zone between a rigid flat (circular) tool and rough chip surface at 700 ℃. (mean contact pressure: a. 0.3 GPa; b. 1.0 GPa; c. 3.0 GPa)

4.5 Validation approach

For the validation, indentation tests can be conducted. A possible approach is the application of a gold layer (thickness < 1 µm) on the smooth tool surface (Fig. 9a). First experiments using a tribometer show that the contact areas after an indentation of a chip (~0.1 GPa) are clearly visible on scanning electron microcopy (SEM) images. Due to the low adhesive force between gold layer and tool elastic as well as plastic deformations might be detected. Even though the surface structure looks comparable to the simulation, the contact area of the experiments is higher than the contact area

of the simulations with 0.3 GPa. This might be attributed to the neglecting chip curvature in the simulation and the non-uniform mechanical properties of the sputtered gold layer.

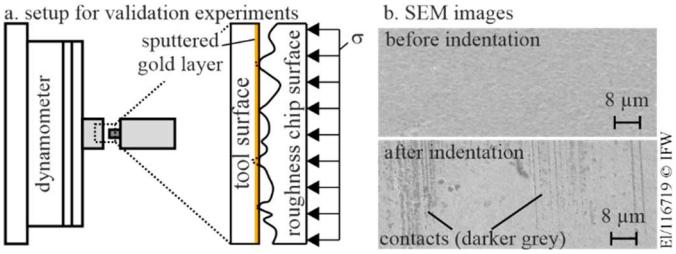

Fig 9: a. possible setup and b. resulting SEM images

5. Conclusions and Outlook

Based on the results, the following conclusions can be drawn:

- CF reduces the contact length on the rake face due to the mechanical loads of the CF acting on the chip.
- The reduced contact length in wet cutting leads to higher local normal stresses up to 3 GPa.
- The real contact area between the rake face and the chip increases with increasing temperature due to reduced elastic modulus.
- The real contact area increases at a higher normal stress. This might also result in a higher contact area in wet cutting. However, in future investigations, a clear differentiation on temperatures in dry and wet cutting has to be carried out.

Even though first basic relations could be shown in the paper, the simulation has to be extended for a more precise modeling of the cutting process. For future modeling, several aspects should be added:

(1) Normal and tangential plastic deformation model;
(2) local friction model and thermal effects;
(3) possible CF penetration and lubrication effects;
(4) coupled with FEM chip formation simulation.

Acknowledgements

The authors appreciate the funding of this work within the Priority Program 2231 “Efficient cooling, lubrication and transportation – coupled mechanical and fluid-dynamical simulation methods for efficient production processes (FLUSIMPRO)” by the German Research Foundation (DFG) – project number 439904924. Liu would like to thank Dr. Binbin Zhang of Schaeffler Greater China for his kind help on the multigrid numerical method.

Appendix A Dimensionless Equations

(1) The gap height equation

$$\overline{H}(\overline{X},\overline{Y}) = \overline{H}_0 + \frac{2}{\pi}\int_{-\infty}^{+\infty}\int_{-\infty}^{+\infty}\frac{\overline{P}(\overline{X}',\overline{Y}')d\overline{X}'d\overline{Y}'}{\sqrt{(\overline{X}-\overline{X}')^2+(\overline{Y}-\overline{Y}')^2}} + \bar{u}_{tool}(\overline{X},\overline{Y}) + \bar{u}_{chip}(\overline{X},\overline{Y}) \quad (A1)$$

(2) The load balance equation

$$\iint \overline{P}(\overline{X},\overline{Y})d\overline{X}d\,\overline{Y} = 2\pi \quad (A2)$$

(3) The complimentary condition

$$\overline{P}(\overline{X},\overline{Y})\overline{H}(\overline{X},\overline{Y}) = 0 \quad (A3)$$

References

[1] Klocke F, Döbbeler B, Lakner T (2018) Influence of the coolant nozzle orientation and size on the tool temperature under highpressure coolant supply using an analogy test bench. Production Engineering – Research and Development 12, p. 473–480
[2] Alagan NT, Hoier P, Zeman P, Klement U, Beno T, Wretland A (2019) Effects of high-pressure cooling in the flank and rake faces of WC tool on the tool wear mechanism and process conditions in turning of alloy 718. Wear 434–435
[3] Klocke F, Krämer A, Sangermann H, Lung D (2012) Thermomechanical tool load during high performance cutting of hard-to-cut materials. Procedia CIRP 1, p. 295–300
[4] Kato S, Yamaguchi K, Yamada M (1972) Stress distribution at the interface between tool and chip in machining. J Eng Ind 94(2) p. 683–689. https:// doi. org/ 10. 1115/1. 34282 29
[5] Childs THC, Mahdi MI, Barrow G (1989) On the stress distributionbetween the chip and tool during metal turning. CIRP Ann 38(1), p. 55–58. https:// doi. org/ 10. 1016/ S0007- 8506(07) 62651-1
[6] Usui E, Kikuchi K, Hoshi, K (1964) The theory of plasticity applied to machining with cut-away tools. Journal of Manufacturing Science and Engineering 86 (2), p. 95-104
[7] Usui E, Takeyama H (1960) A Photoelastic Analysis of Machining Stresses, Journal of Manufacturing Science and Engineering 82(4), p. 303-307
[8] Bergmann B, Grove T (2018) Basic principles for the design of cutting edge roundings. CIRP Ann 67(1) p. 73–78. https:// doi. org/10. 1016/j. cirp. 2018. 04. 019
[9] Bergmann B (2017) Grundlagen zur Auslegung von Schneidkantenverrundungen, Dr.-Ing. Dissertation, Leibniz Universität Hannover
[10] Finnie I, Shaw MC (1957) The friction process in metal cutting. Trans ASME J Eng Ind 79B, p. 1649–1657
[11] Özel T, Biermann D, Enomoto T, Mativenga P (2021) Structured and textured cutting tool surfaces for machining applications. CIRP Ann 70(2), p. 495–518
[12] Saelzer J, Alammari Y, Zabel A, Biermann D, Lee J, Elgeti S (2021) Characterisation and modelling of friction depending on the tool topography and the intermediate medium. Procedia CIRP 102, p.435-440
[13] Williams JA, Tabor D (1977) The Role of Lubricants in Machining, Wear 43, p. 275-292
[14] Denkena B, Krödel A, Ellersiek L (2022) Influence of metal working fluid on chip formation and mechanical loads in orthogonal cutting. Int J Adv Manuf Technol 118(9–10), p. 3005–3013. https://doi. org/ 10. 1007/ s00170- 021- 08164-2
[15] Johnson KL (1987) Contact mechanics. Cambridge university press
[16] Brandt A, Lubrecht AA (1990) Multilevel matrix multiplication and fast solution of integral equations. Journal of Computational Physics 90(2), p. 348-370.
[17] Venner CH, Lubrecht AA (2000) Multi-level methods in lubrication. Elsevier
[18] Liu S, Wang Q, Liu G (2000) A versatile method of discrete convolution and FFT (DC-FFT) for contact analyses. Wear 243(1-2) p. 101-111.
[19] Wang QJ, Sun L, Zhang X, Liu S, Zhu D (2020). FFT-based methods for computational contact mechanics. Frontiers in Mechanical Engineering p. 6-61.
[20] Brnic J, Turkalj G, Canadija M, Lanc D, Brcic M (2015). Study of the effects of high temperatures on the engineering properties of steel 42CrMo4. High Temperature Materials and Processes 34(1), p. 27-34.
[21] Usui E, Shirakashi T, Kitagawa T (1984) Analytical prediction of cutting tool wear. Wear, Vol 100, p. 129 – 151